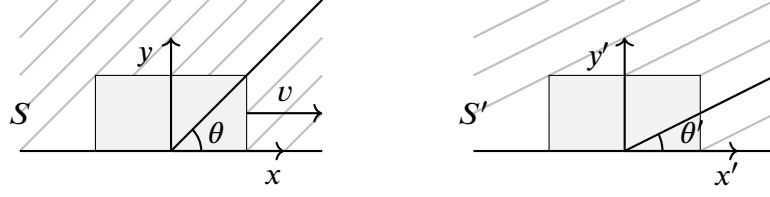# Contents

Figure 1: Path of the rain drops in a frame fixed to the ground and the train.

1   Motivation

This document contains my notes on optical and visual effects resulting from observer motion when the speed of light is finite. The discussed effects are related to the interplay of aberration, Doppler effect, special relativity and the human perception of color. My interest on the topic arose from attempts to solve fascinating problems in the textbook [1] and implementation of aberration correction algorithms.

2   Aberration Formulas

2.1   Classical and Relativistic Aberration

Consider a train cart fixed to the frame S' moving in $+x$-direction with velocity v w.r.t. frame S fixed to the ground. Passenger on the train observes the direction of rain drops from the window. Suppose in S it is raining from direction θ w.r.t. the positive x axis. Then, the path of rain drop falling through $x = y = 0$ can be written

$$
\begin{align}
x(t) &= -u\cos\theta\, t, \tag{1}\\
y(t) &= -u\sin\theta\, t, \tag{2}
\end{align}
$$

where u is the velocity of the rain drop in S. In S', we can express

$$
\begin{align}
x'(t) &= -(u\cos\theta + v)t, \tag{3}\\
y'(t) &= -u(\sin\theta)t. \tag{4}
\end{align}
$$

In S', the angle θ' made by the rain drops w.r.t. positive x axis can be expressed

$$
\tan\theta' = \frac{y'}{x'} = \frac{u\sin\theta}{u\cos\theta + v} = \frac{\tan\theta}{1 + \beta\sec\theta}, \tag{5}
$$

where $\beta = v/u$ and $\sec\theta = 1/\cos\theta$. This classical formula is limited angles in $+x$ direction. More generally,

$$
\theta' = \operatorname{atan2}(\sin\theta, \cos\theta + \beta) \tag{6}
$$

Consider now light in the context of Special Relativity with velocity vector $\boldsymbol{c} = (-c\cos\theta, -c\sin\theta, 0)$. Then, simple application of Lorentz transformation, yields

$$
\begin{align}
x' &= \gamma(x - vt) = -\gamma(c\cos\theta + v)t, \tag{7}\\
y' &= y = -(c\sin\theta)t, \tag{8}
\end{align}
$$

3
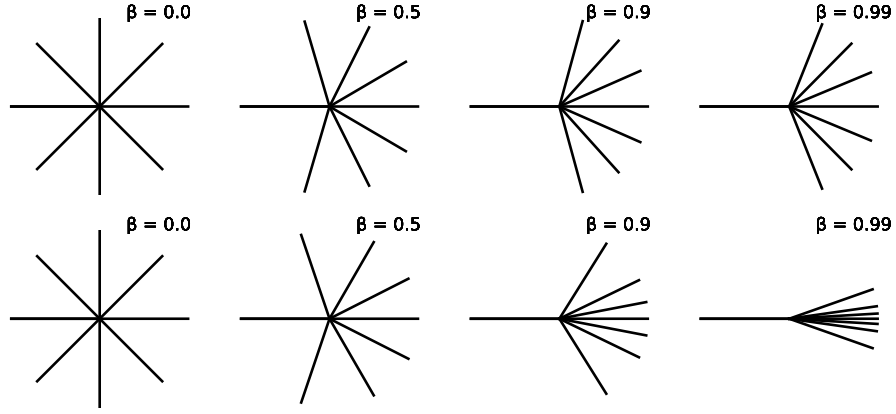
Figure 2: Difference between classical (top) and relativistic (bottom) aberration.

where the **Lorentz factor** is defined

$$\gamma := \frac{1}{\sqrt{1 - v^2/c^2}} = \frac{1}{\sqrt{1 - \beta^2}}. \tag{9}$$

Thus, we obtain the well-known formula for relativistic aberration

$$\tan \theta' = \frac{y'}{x'} = \frac{\tan \theta}{\gamma(1 + \beta \sec \theta)} \tag{10}$$

and the more general expression

$$\theta' = \text{atan2}\left[\sin \theta, \gamma(\cos \theta + \beta)\right] \tag{11}$$

The only difference between classical and relativistic aberration is the Lorentz factor. When β is small, the difference between relativistic and classical results can be usually ignored. At velocities close to the speed of light, the Lorentz factor leads to light sources accumulating around direction of motion (see Figure 2).

2.2 General Vector Expression for Aberration

For practical computations, it is often more convenient to use vectors. Any vector expression for aberration will involve addition of velocity vectors, which is non-trivial in relativistic case.

2.2.1 Classical Aberration

In the classical case, the transformation of velocities is simply

$$\boldsymbol{u}' = \boldsymbol{u} - \boldsymbol{v}. \tag{12}$$

Figure 3: Three-dimensional depiction of the aberration correction for a velocity vector and the associated rotational symmetry.

The direction to target $\hat{\mathbf{s}} = -\boldsymbol{u}'/|\hat{\mathbf{u}}'|$ corrected for aberration is called the **proper direction**. Unlike the relativistic expression $\hat{\mathbf{s}} = -\boldsymbol{u}'/c$, the classical expression for the proper direction needs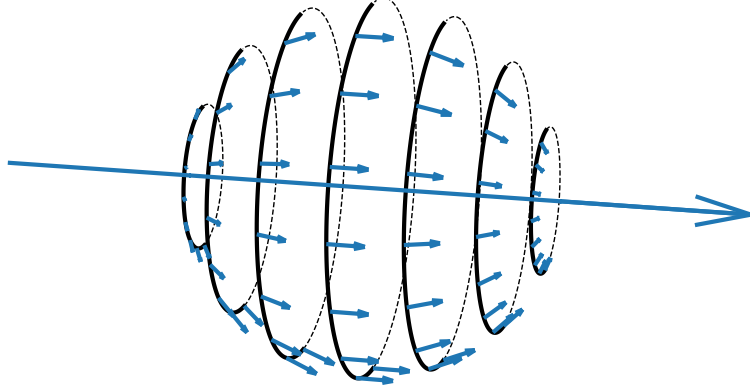 to take into account that classical addition of velocities can lead to velocity of light greater than c. The **uncorrected direction** in both cases can be written $\hat{\mathbf{p}} = -\hat{\mathbf{u}}/c$.

Direct substitution to (12), yields

$$-\hat{\mathbf{s}}|c\hat{\mathbf{p}} + \boldsymbol{v}| = -c\hat{\mathbf{p}} - \boldsymbol{v} \tag{13}$$

and denoting $\boldsymbol{\beta} = \boldsymbol{v}/c$, we obtain the classical vector expression for proper direction

$$\boxed{\hat{\mathbf{s}} = \frac{\hat{\mathbf{p}} + \boldsymbol{v}/c}{|\hat{\mathbf{p}} + \boldsymbol{v}/c|} = \frac{\hat{\mathbf{p}} + \boldsymbol{\beta}}{|\hat{\mathbf{p}} + \boldsymbol{\beta}|}} . \tag{14}$$

2.2.2 General Lorentz Transformation of Velocities

Let S' move w.r.t. S with velocity $\boldsymbol{v}$ and denote

$$\boldsymbol{u} := \frac{d\boldsymbol{r}}{dt}, \quad \boldsymbol{u}' := \frac{d\boldsymbol{r}'}{dt'}, . \tag{15}$$

Then, the Lorentz transformation will only affect coordinates along the direction of the velocity. That is, parallel and perpendicular components of $d\boldsymbol{r}$ transform as

$$d\boldsymbol{r}'_{\|} = \gamma \left(d\boldsymbol{r}_{\|} - \boldsymbol{v}\, dt \right) \tag{16}$$
$$d\boldsymbol{r}'_{\perp} = d\boldsymbol{r}_{\perp}. \tag{17}$$

The time transforms as

$$dt' = \gamma \left(dt - \frac{\boldsymbol{v} \cdot d\boldsymbol{r}}{c^2} \right) = \gamma \left(1 - \frac{\boldsymbol{v} \cdot \boldsymbol{u}}{c^2} \right) dt. \tag{18}$$

5

Now we can expand the components of velocity in S'

$$u'_\| = \frac{dr'_\|}{dt'} = \frac{\gamma(r_\| - v\,dt)}{\gamma(1 - v\cdot u/c^2)dt} = \frac{u_\| - v}{1 - v\cdot u/c^2} \tag{19}$$

$$u'_\perp = \frac{dr'_\perp}{dt'} = \frac{dr_\perp}{\gamma(1 - v\cdot u/c^2)dt} = \frac{u_\perp}{\gamma(1 - v\cdot u/c^2)} \tag{20}$$

The velocity in S' can be expanded using

$$u_\| = \frac{u\cdot v}{v^2}v, \quad u_\perp = u - u_\| = u - \frac{u\cdot v}{v^2}v \tag{21}$$

leading to

$$u' = u'_\| + u'_\perp \tag{22}$$

$$= \frac{u_\| - v + u_\perp/\gamma}{1 - v\cdot u/c^2} \tag{23}$$

$$= \frac{1}{1 - v\cdot u/c^2}\left[\frac{u\cdot v}{v^2}v - v + \frac{1}{\gamma}\left(u - \frac{u\cdot v}{v^2}v\right)\right] \tag{24}$$

$$= \frac{1}{1 - v\cdot u/c^2}\left\{\frac{1}{\gamma}u + v\left[\frac{u\cdot v}{v^2}\left(1 - \frac{1}{\gamma}\right) - 1\right]\right\} \tag{25}$$

$$= \frac{1}{\gamma(1 - v\cdot u/c^2)}\left[u + v\left(\frac{u\cdot v}{v^2}(\gamma - 1) - \gamma\right)\right]. \tag{26}$$

2.2.3 Relativistic Aberration

Let $\hat{\mathbf{n}} = u/c$ be the direction of light propagation and $\hat{\mathbf{s}} = -u'/c$ be the (relativistic) proper direction. Substitution to the General Lorentz Transformation for velocities (26) then yields

$$-c\hat{\mathbf{s}} = \frac{1}{\gamma(1 - \hat{\mathbf{n}}\cdot v/c)}\left\{c\hat{\mathbf{n}} + v\left[\frac{c}{v^2}(\hat{\mathbf{n}}\cdot v)(\gamma - 1) - \gamma\right]\right\} \tag{27}$$

or

$$\hat{\mathbf{s}} = \frac{1}{\gamma(1 - \hat{\mathbf{n}}\cdot v/c)}\left\{-\hat{\mathbf{n}} + v\left[\frac{\gamma}{c} - \frac{1}{v^2}(\hat{\mathbf{n}}\cdot v)(\gamma - 1)\right]\right\} \tag{28}$$

$$= \frac{1}{\gamma(1 - \hat{\mathbf{n}}\cdot v/c)}\left\{-\hat{\mathbf{n}} + v\frac{\gamma}{c}\left[1 - \frac{c}{v^2}(\hat{\mathbf{n}}\cdot v)\frac{\gamma - 1}{\gamma}\right]\right\} \tag{29}$$

$$= \frac{1}{\gamma(1 - \hat{\mathbf{n}}\cdot v/c)}\left[-\hat{\mathbf{n}} + v\frac{\gamma}{c}\left(1 - \frac{\gamma}{\gamma + 1}\frac{v\cdot\hat{\mathbf{n}}}{c}\right)\right], \tag{30}$$

where in the last step we have used

$$\frac{\gamma - 1}{\gamma\beta^2} = \frac{\gamma - 1}{\gamma(1 - \gamma^{-2})} = \frac{\gamma^2 - \gamma}{\gamma^2 - 1} = \gamma\frac{\gamma - 1}{(\gamma - 1)(\gamma + 1)} = \frac{\gamma}{\gamma + 1} \tag{31}$$

$$\Rightarrow \frac{c}{v^2}\frac{\gamma - 1}{\gamma}(v\cdot\hat{\mathbf{n}}) = \frac{1}{c}\frac{\gamma - 1}{\gamma\beta^2}(v\cdot\hat{\mathbf{n}}) \tag{32}$$

6

Denoting $\boldsymbol{\beta} = \boldsymbol{v}/c$, we obtain expression for the proper direction

$$\hat{\mathbf{s}} = \frac{1}{\gamma(1 - \hat{\mathbf{n}} \cdot \boldsymbol{\beta})} \left[-\hat{\mathbf{n}} + \gamma\boldsymbol{\beta} \left(1 - \frac{\gamma}{\gamma + 1} \boldsymbol{\beta} \cdot \hat{\mathbf{n}} \right) \right] \tag{33}$$

Let $\boldsymbol{p} = -\hat{\mathbf{n}}$ be the uncorrected direction. Then (33) can be expressed

$$\boxed{\hat{\mathbf{s}} = \frac{1}{\gamma(1 + \hat{\mathbf{p}} \cdot \boldsymbol{\beta})} \left[\hat{\mathbf{p}} + \gamma\boldsymbol{\beta} \left(1 + \frac{\gamma}{\gamma + 1} \boldsymbol{\beta} \cdot \hat{\mathbf{p}} \right) \right] .} \tag{34}$$

2.3 Series Expansion of Aberration Correction

2.3.1 Classical Aberration

Cross product of (14) with uncorrected direction $\boldsymbol{p}$, yields

$$\sin \Delta\theta \, \hat{\mathbf{n}} = \hat{\mathbf{p}} \times \hat{\mathbf{s}} = \frac{\hat{\mathbf{p}} \times \hat{\mathbf{p}} + \hat{\mathbf{p}} \times \boldsymbol{\beta}}{|\hat{\mathbf{p}} + \boldsymbol{\beta}|} = \frac{\hat{\mathbf{p}} \times \boldsymbol{\beta}}{|\hat{\mathbf{p}} + \boldsymbol{\beta}|} = \frac{||\hat{\mathbf{p}}|| \, ||\boldsymbol{\beta}|| \sin\theta \, \hat{\mathbf{n}}}{|\hat{\mathbf{p}} + \boldsymbol{\beta}|} = \frac{\beta \sin\theta \, \hat{\mathbf{n}}}{\sqrt{1 + 2\beta\cos\theta + \beta^2}}, \tag{35}$$

where we have used

$$\begin{aligned}
||\hat{\mathbf{p}} + \boldsymbol{\beta}||^2 &= (||\hat{\mathbf{p}}|| + ||\boldsymbol{\beta}|| \cos\theta)^2 + \beta^2 \sin^2\theta && \tag{36} \\
&= 1 + 2\beta\cos\theta + \beta^2\cos^2\theta + \beta^2\sin^2\theta && \tag{37} \\
&= 1 + 2\beta\cos\theta + \beta^2. && \tag{38}
\end{aligned}$$

According to generalized binomial theorem

$$\frac{1}{\sqrt{1 + x}} = \sum_{k=0}^{\infty} \binom{-1/2}{k} x^n \approx 1 - \frac{1}{2}x + \frac{3}{8}x^2 - \frac{5}{16}x^3 + \dots \tag{39}$$

Substitution of $x = 2\beta\cos\theta + \beta^2$, yields

$$\begin{aligned}
\frac{1}{\sqrt{1 + 2\beta\cos\theta + \beta^2}} &\approx 1 - \frac{1}{2}(2\beta\cos\theta + \beta^2) + \frac{3}{8}(2\beta\cos\theta + \beta^2)^2 && \tag{40} \\
&= 1 - \cos\theta\beta + \left(\frac{3}{2}\cos^2\theta - \frac{1}{2} \right)\beta^2 + \frac{3}{2}\cos\theta\beta^3 + \frac{3}{8}\beta^4 && \tag{41}
\end{aligned}$$

and if we ignore everything above fourth power of β, we can expand

$$\sin\Delta\theta \approx \beta\sin\theta - \frac{1}{2}\beta^2\sin 2\theta + \frac{1}{8}\beta^3(3\sin 3\theta - \sin\theta) + \frac{3}{4}\beta^4\sin 2\theta \tag{42}$$

Note that when such a series is expressed as a linear combination of sinusoidal terms, it is obvious that $\Delta\theta$ antisymmetric w.r.t. θ and zero at $\theta = 0$. The above formula also produces a positive $\Delta\theta$ with positive θ, which is incorrect. In most applications, where β is small, we can approximate

$$\boxed{\Delta\theta \approx \sin\Delta\theta \approx -\beta\sin\theta + \frac{1}{2}\beta^2\sin 2\theta.} \tag{43}$$

2.3.2 Relativistic Aberration

Cross product of (34) with uncorrected direction $\hat{\mathbf{p}}$, yields

$$||\hat{\mathbf{s}}|| \, ||\hat{\mathbf{p}}|| \sin \Delta\theta \hat{\mathbf{n}} = \hat{\mathbf{s}} \times \hat{\mathbf{p}} \tag{44}$$

$$= \frac{\boldsymbol{\beta} \times \hat{\mathbf{p}}}{1 + \hat{\mathbf{p}} \cdot \boldsymbol{\beta}} \left(1 + \frac{\gamma}{\gamma + 1} \boldsymbol{\beta} \cdot \hat{\mathbf{p}} \right) \tag{45}$$

$$= \frac{\beta \sin \theta}{1 + \beta \cos \theta} \left(1 + \frac{\gamma}{\gamma + 1} \beta \cos \theta \right) \hat{\mathbf{n}}. \tag{46}$$

To obtain a series expansion for $\sin \Delta\theta$, note that:

$$\frac{1}{1 + \beta \cos \theta} = \sum_{k=0}^{\infty} (-1)^k \beta^k \cos^k \theta \approx 1 - \beta \cos \theta + \beta^2 \cos^2 \theta, \tag{47}$$

$$\frac{\gamma}{\gamma + 1} = \frac{1}{1 + \sqrt{1 - \beta^2}} = \frac{1}{1 + \sqrt{1 - \beta^2}} \frac{1 - \sqrt{1 - \beta^2}}{1 - \sqrt{1 - \beta^2}} = \frac{1 - \sqrt{1 - \beta^2}}{\beta^2}, \tag{48}$$

$$\sqrt{1 - \beta^2} = \sum_{k=0}^{\infty} \binom{1/2}{k} (-1)^k \beta^{2k} \approx 1 - \frac{1}{2}\beta^2 + \frac{1}{8}\beta^4. \tag{49}$$

Thus, we can also expand

$$\frac{1 - \sqrt{1 - \beta^2}}{\beta^2} \approx \frac{1}{\beta^2} \left[1 - \left(1 - \frac{1}{2}\beta^2 + \frac{1}{8}\beta^4 \right) \right] = \frac{1}{2} - \frac{1}{8}\beta^2, \tag{50}$$

$$\beta \sin \theta \left(1 + \frac{\gamma}{\gamma + 1} \beta \cos \theta \right) \approx \beta \sin \theta + \beta^2 \sin \theta \cos \theta \left(\frac{1}{2} - \frac{1}{8}\beta^2 \right) \approx \beta \sin \theta + \frac{1}{4}\beta^2 \sin 2\theta \tag{51}$$

and finally

$$\sin \Delta\theta \approx (1 - \beta \cos \theta) \left(\beta \sin \theta + \frac{1}{4}\beta^2 \sin 2\theta \right) \tag{52}$$

$$\approx \beta \sin \theta - \beta^2 \sin \theta \cos \theta + \frac{1}{4}\beta^2 \sin 2\theta \tag{53}$$

Thus, again noting the sign, we obtain the approximation

$$\boxed{\Delta\theta \approx \sin \Delta\theta \approx -\beta \sin \theta + \frac{1}{4}\beta^2 \sin 2\theta.} \tag{54}$$

2.3.3 Accuracy

The difference in the quadratic term between (54) and (43) suggests that the linear approximation can be more preferrable than the quadratic classical approximation. Comparison with two values of θ is shown in Figure 4. Worst case (w.r.t. θ) relative errors are shown in Figure 5.

The linear approximation is usually sufficient for most purposes in astrometry: For example, if Earth's speed along it's orbit is about 30 km/s or $\beta \approx 10^{-4}$, the maximum relative error from linear and quadratic approximations are on the scale of 10^{-4} and 10^{-8}, respectively. If the maximum aberration is around 20", this corresponds to absolute errors around 2 mas and 0.2 μas, respectively.
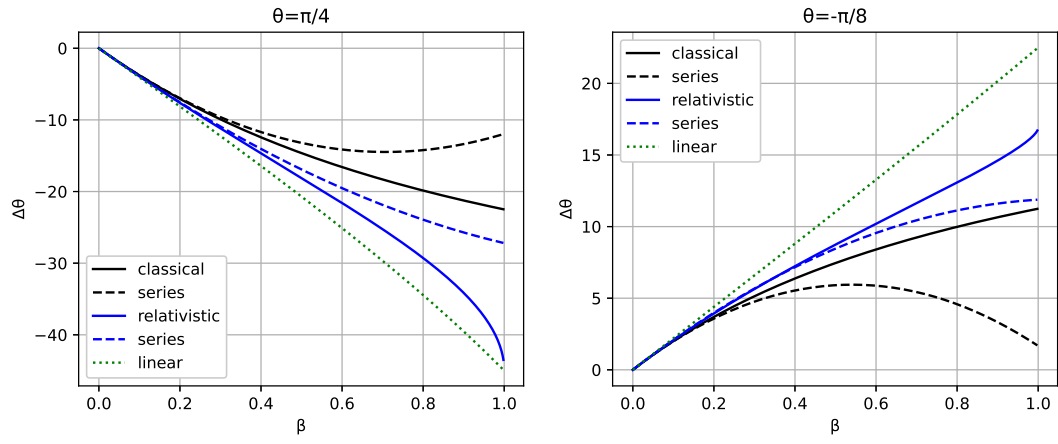
Figure 4: Linear and quadratic approximation of classical and relativistic aberration.
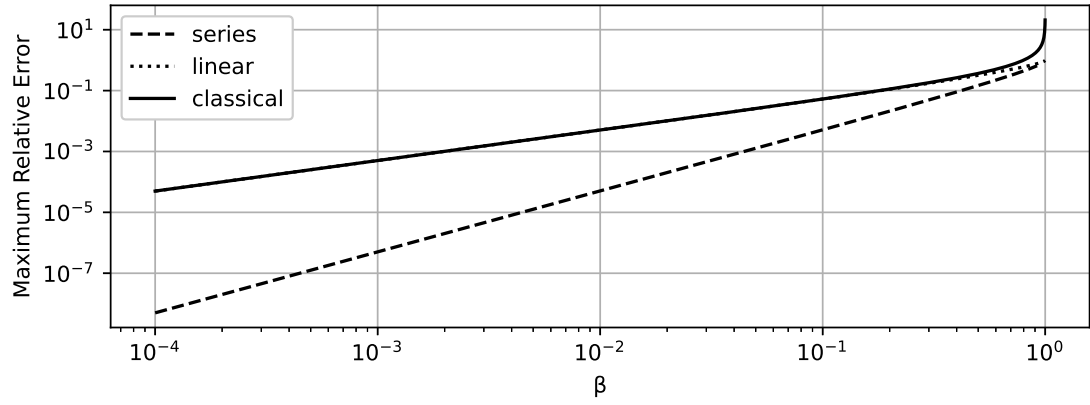

Figure 5: Maximum aberration error with respect to the exact relativistic formula.

2.4 Spherical Coordinates

We expand uncorrected direction

$$\hat{\mathbf{p}} = \begin{bmatrix} \cos\delta\cos\alpha \\ \cos\delta\sin\alpha \\ \sin\delta \end{bmatrix}, \tag{55}$$

where δ and α are the declination and the right ascension, respectively (in appropriate frames). Then, unit vectors along the declination and right ascension coordinates can be written

$$\hat{\mathbf{e}}_\delta = \frac{\partial\hat{\mathbf{p}}}{\partial\delta} = \begin{bmatrix} -\sin\delta\cos\alpha \\ -\sin\delta\sin\alpha \\ \cos\delta \end{bmatrix}, \quad \hat{\mathbf{e}}_\alpha = \frac{1}{\cos\delta}\frac{\partial\hat{\mathbf{p}}}{\partial\alpha} = \begin{bmatrix} -\sin\alpha \\ \cos\alpha \\ 0 \end{bmatrix}. \tag{56}$$

Thus, for small $\hat{\mathbf{s}} - \hat{\mathbf{p}}$, we can approximate

$$\Delta\delta \quad = \quad (\hat{\mathbf{s}} - \hat{\mathbf{p}}) \cdot \hat{\mathbf{e}}_\delta \tag{57}$$

$$\cos\delta\Delta\alpha \quad = \quad (\hat{\mathbf{s}} - \hat{\mathbf{p}}) \cdot \hat{\mathbf{e}}_\alpha \tag{58}$$

For small v/c, we can approximate from (14)

$$\hat{\mathbf{s}} - \hat{\mathbf{p}} \approx \boldsymbol{\beta}. \tag{59}$$

Thereafter, we obtain

$$\Delta\delta \quad = \quad \hat{\mathbf{e}}_\delta \cdot \boldsymbol{\beta} = -\beta_x\sin\delta\cos\alpha - \beta_y\sin\delta\sin\alpha + \beta_z\cos\delta \tag{60}$$

$$\cos\delta\Delta\alpha \quad = \quad \hat{\mathbf{e}}_\alpha \cdot \boldsymbol{\beta} = -\beta_x\sin\alpha + \beta_y\cos\alpha. \tag{61}$$
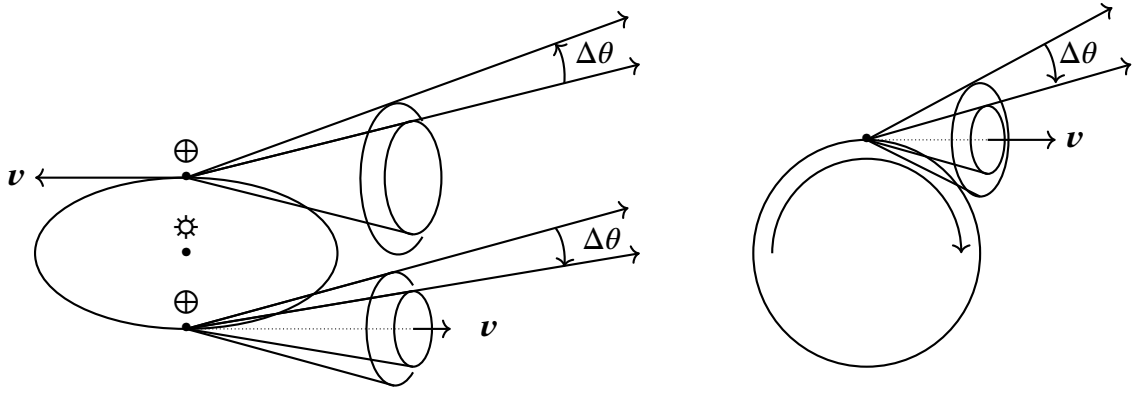
Figure 6: Annual aberration correction for a planet orbiting the Sun (left). Diurnal aberration correction for an observer on the surface of a rotating planet (right). The cones depict rotational symmetry in the correction.

3   Stellar Aberration

Stellar aberration refers to the apparent change in the position of a stellar object due to velocity of the observer. For an observer fixed to the surface of a rotating planet, the stellar aberration may involve:

- **Annual aberration** resulting from the motion of the planet around the barycenter of the solar system. For Earth, the velocity of 29.79 km/s around the barycenter of the solar system amounts to a maximum correction on 20.496 arcseconds.

- **Diurnal aberration** resulting from the rotation of the planet. At the equator, Earth rotates approximately with the tangential velocity of 465 meters per second, which amounts to a maximum correction of 0.32 arcseconds.

- **Secular aberration** resulting from the approximately uniform motion of the solar system around the center of the galaxy. For our solar system, this velocity. is about 220 km/s and amounts to a maximum correction of 150". However, since the velocity changes very slowly, the effect is included in the catalogued positions and is not corrected.

- **Planetary aberration** resulting from both the motion of the observer and the movement of the observed body.

Aberration can also result from the observer moving w.r.t. the surface of the planet. For example, a fighter jet or a missile can travel at speeds higher than the rotation speed of Earth. However, this effect is likely always small enough to be neglected in technical applications. For a satellite on LEO moving at 8 km/s w.r.t. inertial frame centered on Earth, the maximum aberration is around 5.5 arcseconds.

The expressions developed in the previous section apply to all types of aberration.

3.1 Linear Approximation in Spherical Coordinates

3.1.1 Annual Aberration

For elliptic orbits, the velocity and distance from the center can be expressed

$$v = \sqrt{\mu \left(\frac{2}{r} - \frac{1}{a} \right)}, \quad r = \frac{a(1 - e^2)}{1 + e \cos f}. \tag{62}$$

At perihelion and aphelion $f = 0$ and $f = 180°$, respectively corresponding to maximum and minimum velocities

$$v_{max} = \sqrt{\frac{\mu}{a} \left(\frac{1 + e}{1 - e} \right)}, \quad v_{min} = \sqrt{\frac{\mu}{a} \left(\frac{1 - e}{1 + e} \right)}. \tag{63}$$

For Earth's orbit around the Sun, we can substitue $\mu = 1.32712440042 \cdot 10^{20}\,\mathrm{m}^3\mathrm{s}^{-2}$, $e = 0.01671022$ and $a = 1.495980229607128 \cdot 10^{11}$ m leading to

$$v_{max} = 30286.614 \text{ m/s}, \quad v_{min} = 29291.058 \text{ m/s}, \quad v_{avg} = 29790.915 \text{ m/s}. \tag{64}$$

The **constant of aberration** κ is the maximum possible displacement of a distant object due to aberration and can be approximated $\kappa \approx v/c$. Correspondingly, we obtain

$$\kappa_{max} = 20.838'', \quad \kappa_{min} = 20.153'', \quad \kappa_{avg} = 20.497''. \tag{65}$$

To obtain geometric intuition about annual aberration throughout the year, consider a circular orbit with zero inclination. That is,

$$\boldsymbol{\beta}(t) = \beta(\cos \omega t, \sin \omega t, 0). \tag{66}$$

Substitution to (60) and (61), yields

$$\Delta \delta = -\beta \sin \delta \cos \alpha \cos \omega t - \beta \sin \delta \sin \alpha \sin \omega t \tag{67}$$
$$\cos \delta \Delta \alpha = -\beta \sin \alpha \cos \omega t + \beta \cos \alpha \sin \omega t. \tag{68}$$

Suppose $\alpha = 0$. Then, the above simplifies to

$$\Delta \delta = -\beta \sin \delta \cos \omega t, \tag{69}$$
$$\cos \delta \Delta \alpha = \beta \sin \omega t. \tag{70}$$

That is, annual aberration will lead to a displacement shaped like an ellipse with a period of one orbit (see Figure 7).

3.1.2 Diurnal Aberration

The velocity of the observer on the surface of Earth can be written
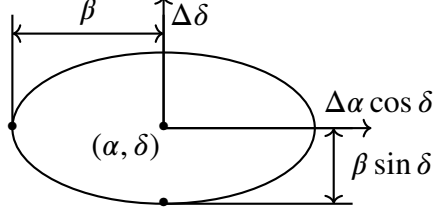
$$v = \omega(R + h) \cos \phi, \tag{71}$$

12

Figure 7: Elliptical shape of abberation correction w.r.t. the uncorrected position.

where R, h and ϕ are the radius of Earth, altitude of the observer above the surface of Earth and the latitude. Consequently, the aberration can be approximated

$$\Delta\theta \approx \beta \approx \frac{\omega(R+h)}{c}\cos\phi. \tag{72}$$

Substitution of $R = 6371$ km, $\omega = 2\pi/86164.0905$ s yields at the equator

$$\Delta\theta \approx -0.3196''. \tag{73}$$

The velocity is always approximately towards the east corresponding to the x-axis in the ENU frame. That is, substituting $\boldsymbol{\beta} = \beta\hat{\mathbf{x}}$ to (60) and (61), yields

$$\Delta\delta \quad = \quad -\beta\sin\delta\cos\alpha \tag{74}$$
$$\cos\delta\Delta\alpha \quad = \quad -\beta\sin\alpha. \tag{75}$$

The notation above is misleading in the sense δ and α do not refer to declination and right ascension. To obtain an expression in terms of elevation and azimuth, substitute for $a = \delta$ and $\alpha = 90° - \phi$ to obtain

$$\Delta a \quad = \quad -\beta\sin a\sin\phi, \tag{76}$$
$$\cos a\Delta\phi \quad = \quad \beta\cos\phi. \tag{77}$$

For $\phi = 90°$ (east), we obtain $\Delta a = -\beta\sin a$ and for $a = 0$, we obtain $\Delta\phi = \beta\cos\phi = -\beta\sin(\phi - 90°)$, which is consistent with (54).

3.2 Planetary Aberration and Light-Time

The travel time of light between target and the observer is called **light-time** and denoted τ. When the direction to target changes significantly during light-time, this requires a correction. The relative apparent position to target can be expressed

$$\boldsymbol{p}(t) = \boldsymbol{u}_B(t - \tau) - \boldsymbol{E}_B(t), \tag{78}$$

13

where $\boldsymbol{u}_B$ and $\boldsymbol{E}_B$ are the barycentric positions of the target and the observer. Application of (14) yields

$$
\begin{align}
\boldsymbol{s}(t) &= \boldsymbol{p}(t) + \beta|\boldsymbol{p}| \tag{79}\\
&= \boldsymbol{u}_B(t-\tau) - \boldsymbol{E}_B(t) + \frac{|\boldsymbol{p}|}{c}\dot{\boldsymbol{E}}_B(t) \tag{80}\\
&= \boldsymbol{u}_B(t-\tau) - \boldsymbol{E}_B(t) + \tau\dot{\boldsymbol{E}}_B(t) \tag{81}\\
&\approx \boldsymbol{u}_B(t-\tau) - \boldsymbol{E}_B(t-\tau). \tag{82}
\end{align}
$$

That is, correcting for planetary aberration at t with classical approximation (14) is equivalent to the computation the uncorrected direction to target at $t-\tau$. Note that this does not take into account the diurnal aberration.

3.3   Practical Computation

The positions of stars are typically catalogued w.r.t. the Solar System Barycenter (SSB) so that secular aberration is already included in the catalogued positions. Thus, to compute the aberration correction for an observer, we need to compute the velcoity vector of the observer w.r.t. the SSB. For an observer on Earth, this velocity is the sum of the orbital velocity of the Earth around the SSB and the rotational velocity of the topocentric position of the observer around the geocenter (GEO) of Earth. Thereafter, (14) and (34) can be applied in any topocentric frame centered on the observer position.

3.3.1   Transformations Between Frames

Let us denote the position and velocity coordinate vector for target C in frame with orientation A and origin B with $\boldsymbol{r}^B_{C(A)}$ and $\boldsymbol{v}^B_{C(A)}$. Omission of C, A or B in an expression signifies that the expression applies for all targets, orientations or origins, respectively. Then, if R^a_A is the rotation matrix from orientation a to A, we can write

$$
\boldsymbol{r}_{(A)} = R^a_A \boldsymbol{r}_{(a)} \quad \Leftrightarrow \quad \boldsymbol{r}^B_{C(A)} = R^a_A \boldsymbol{r}^B_{C(a)} \quad \forall B, C. \tag{83}
$$

Similarly, for any two origins B and b

$$
\boldsymbol{r}^B = \boldsymbol{r}^b - \boldsymbol{r}^b_B \quad \Leftrightarrow \quad \boldsymbol{r}^B_{C(A)} = \boldsymbol{r}^b_{C(A)} - \boldsymbol{r}^b_{B(A)} \quad \forall A, C. \tag{84}
$$

The equation (83) does not apply to velocity vectors unless the rotation matrix is constant w.r.t. time. More generally, we can expand

$$
\boldsymbol{v}_{(A)} = \frac{d}{dt}\boldsymbol{r}_{(A)} = \frac{d}{dt}\left(R^a_A \boldsymbol{r}_{(a)}\right) = \dot{R}^a_A \boldsymbol{r}_{(a)} + R^a_A \boldsymbol{v}_{(a)}, \tag{85}
$$

where the $\dot{R}^a_A \boldsymbol{r}_{(a)}$ corresponds to velocity component from the rotation of $\boldsymbol{r}_{(a)}$ w.r.t. the origin.

3.3.2 Expansion of the Observer Velocity

The position and velocity vectors w.r.t. origins at the GEO and the SSB can be related by

$$r^{GEO} = r^{SSB} - r^{SSB}_{GEO}, \qquad (86)$$

$$v^{GEO} = v^{SSB} - v^{SSB}_{GEO}, \qquad (87)$$

where v^{SSB}_{GEO} is the orbital velocity of the geocenter w.r.t. the SSB. The rotation of the Earth can be expressed via the coordinate transform between inertial True-of-Date (ToD) and Pseudo-Earth-Fixed (PEF) frames

$$r^{GEO}_{(PEF)} = R^{TOD}_{PEF} r^{GEO}_{(TOD)} \quad : \quad R^{TOD}_{PEF} = \begin{bmatrix} \cos GAST & \sin GAST & 0 \\ -\sin GAST & \cos GAST & 0 \\ 0 & 0 & 1 \end{bmatrix}, \qquad (88)$$

$$r^{GEO}_{(TOD)} = R^{PEF}_{TOD} r^{GEO}_{(PEF)} \quad : \quad R^{PEF}_{TOD} = \begin{bmatrix} \cos GAST & -\sin GAST & 0 \\ \sin GAST & \cos GAST & 0 \\ 0 & 0 & 1 \end{bmatrix}. \qquad (89)$$

where GAST is the Greenwich Apparent Sidereal Time. The corresponding velocities can be expanded

$$v^{GEO}_{(PEF)} = R^{TOD}_{PEF} v^{GEO}_{(TOD)} + \dot{R}^{TOD}_{PEF} r^{GEO}_{(TOD)}, \qquad (90)$$

$$v^{GEO}_{(TOD)} = R^{PEF}_{TOD} v^{GEO}_{(PEF)} + \dot{R}^{PEF}_{TOD} r^{GEO}_{(PEF)}, \qquad (91)$$

where

$$\dot{R}^{TOD}_{PEF} = \frac{dGAST}{dt} \begin{bmatrix} -\sin GAST & \cos GAST & 0 \\ -\cos GAST & -\sin GAST & 0 \\ 0 & 0 & 0 \end{bmatrix} \qquad (92)$$

$$\dot{R}^{PEF}_{TOD} = \frac{dGAST}{dt} \begin{bmatrix} -\sin GAST & -\cos GAST & 0 \\ \cos GAST & -\sin GAST & 0 \\ 0 & 0 & 0 \end{bmatrix}. \qquad (93)$$

For computation of diurnal aberration amounting to less than 0.32 arcseconds, we can approximate the time derivative of GAST using the length of a sidereal day

$$\frac{dGAST}{dt} \approx \frac{2\pi \text{ rad}}{86164.0905 \ s} \approx 7.2921159 \cdot 10^{-5} \text{rad/s} \approx 15.04107°/h. \qquad (94)$$

The velocity of the observer w.r.t. the SSB can be expressed

$$v^{SSB}_{(ECL)} = v^{SSB}_{GEO,(ECL)} + R^{TOD}_{ECL} v^{GEO}_{(TOD)} \qquad (95)$$

$$= v^{SSB}_{GEO,(ECL)} + R^{TOD}_{ECL} \left(R^{PEF}_{TOD} v^{GEO}_{(PEF)} + \dot{R}^{PEF}_{TOD} r^{GEO}_{(PEF)} \right). \qquad (96)$$

The position of the observer $r^{GEO}_{(PEF)} = R^{EFI}_{PEF} r^{GEO}_{(EFI)}$, where $r^{GEO}_{(EFI)}$ can obtained from geodetic position on WGS84. For an observer that is stationary w.r.t. surface of Earth $v^{GEO}_{(PEF)} = \mathbf{0}$.

15

Aberration corrections (14) and (34) can be applied in the ecliptic frame centered on the SSB or the topocentric ENU frame of the observer. Application in an ENU frame requires rotation

$$R_{ENU}^{ECL} \boldsymbol{v}_{(ECL)}^{SSB} = R_{ENU}^{ECL} \boldsymbol{v}_{GEO,(ECL)}^{SSB} + R_{ENU}^{TOD} \left(R_{TOD}^{PEF} \boldsymbol{v}_{(PEF)}^{GEO} + \dot{R}_{TOD}^{PEF} \boldsymbol{r}_{(PEF)}^{GEO} \right). \tag{97}$$

Note that since the aberration relates to the velocity difference between the observer and the SSB in an inertial frame, it is not appropriate to transfer the velocity of SSB to a topocentric frame, where it would rotate around the observer location at very high speed.
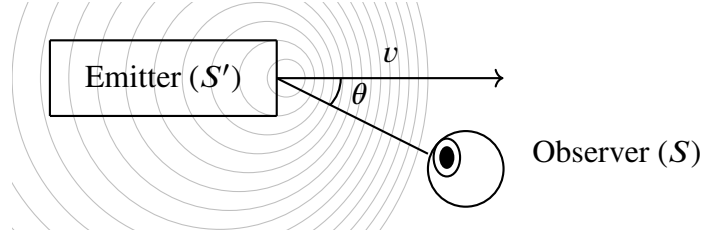
Figure 8: Geometry associated to Doppler Effect.

4 Doppler Effect

4.1 Classical and Relativistic Doppler Effect

Consider a light source fixed to an inertial frame S' moving with velocity v w.r.t. an observer fixed to an inertial frame S (see Figure 8). Suppose that the direction of movement makes the angle θ w.r.t. direction to the observer. Let $\boldsymbol{v} = v\hat{\mathbf{x}}$ and represent the wavefront towards the observer with phase angle

$$\phi(\boldsymbol{x}, t) = A\cos(\boldsymbol{k} \cdot \boldsymbol{x} - \omega t), \tag{98}$$

where the wave vector satisfies

$$\boldsymbol{k} = k\cos\theta\,\hat{\mathbf{x}} + k\sin\theta\,\hat{\mathbf{y}}. \tag{99}$$

Substitution of $kx - \omega t = 0$ yields in vacuum $x = \omega t/k = ct$ and $k = \omega/c$.

The phase angle ϕ in the frames S and S' can be related by the Galilean transformation

$$
\begin{aligned}
t &= t' & (100) \\
x &= x' + vt & (101) \\
y &= y' & (102) \\
z &= z' & (103)
\end{aligned}
$$

with the expansion

$$
\begin{aligned}
\boldsymbol{k} \cdot \boldsymbol{x} - \omega t &= kx\cos\theta + ky\sin\theta - \omega t & (104) \\
&= k(x' + vt)\cos\theta + ky\sin\theta - \omega t & (105) \\
&= kx'\cos\theta + ky'\sin\theta - \omega(1 - \beta\cos\theta) & (106) \\
&= \boldsymbol{k}' \cdot \boldsymbol{x}' - \omega't & (107)
\end{aligned}
$$

Thus, we obtain the expression for **classical Doppler Effect**

$$\boxed{\omega = \frac{\omega'}{1 - \beta\cos\theta}, \quad k' = k.} \tag{108}$$

17

In the relativistic case, we replace the Galilean transformation with the Lorentz transformation

$$t = \gamma(t' + \beta x'/c) \tag{109}$$
$$x = \gamma(x' + vt) \tag{110}$$
$$y = y' \tag{111}$$
$$z = z'. \tag{112}$$

Now we can expand

$$
\begin{aligned}
\boldsymbol{k} \cdot \boldsymbol{x} - \omega t &= k\gamma(x' + vt')\cos\theta + ky\sin\theta - \omega\gamma(t' + \beta x'/c) \tag{113} \\
&= \gamma(k\cos\theta - \omega\beta/c)x' + ky\sin\theta - \gamma(\omega - kv\cos\theta))t' \tag{114} \\
&= \gamma k(\cos\theta - \beta)x' + ky'\sin\theta - \gamma\omega(1 - \beta\cos\theta)t' \tag{115} \\
&= \boldsymbol{k}' \cdot \boldsymbol{x}' - \omega't' \tag{116}
\end{aligned}
$$

and obtain the expression for **relativistic Doppler Effect**

$$\boxed{\omega = \frac{\omega'}{\gamma(1 - \beta\cos\theta)}, \quad \boldsymbol{k}' = \gamma k(\cos\theta - \beta)\hat{\boldsymbol{x}} + k\sin\theta\hat{\boldsymbol{y}}.} \tag{117}$$

The transformation of the wave vector corresponds to the relativistic aberration correction.

4.2 Interpretation

4.2.1 Longitudal Doppler Effect

The special cases relating to longitudal motion are depicted in Figure 9. When $\theta = 180°$ and $\theta = 0°$, we can expand

$$\frac{\omega}{\omega'} = \frac{1}{\gamma(1 + \beta)} = \frac{\sqrt{(1 + \beta)(1 - \beta)}}{1 + \beta} = \sqrt{\frac{1 - \beta}{1 + \beta}} \leq 1 \tag{118}$$

$$\frac{\omega}{\omega'} = \frac{1}{\gamma(1 - \beta)} = \frac{\sqrt{(1 + \beta)(1 - \beta)}}{1 - \beta} = \sqrt{\frac{1 + \beta}{1 - \beta}} \geq 1 \tag{119}$$
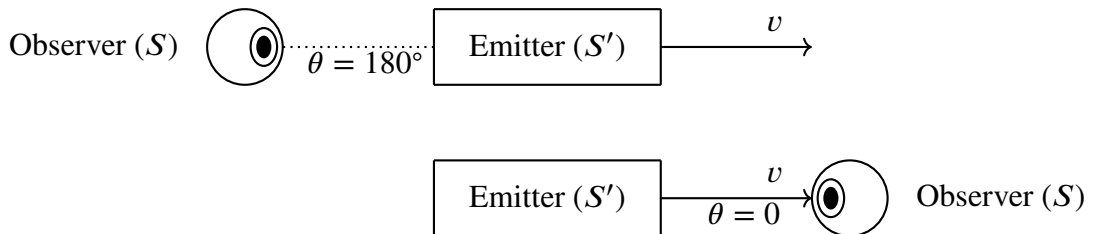
respectively.

Figure 9: Geometry associated to maximal redshift (top) and maximal blueshift (below).
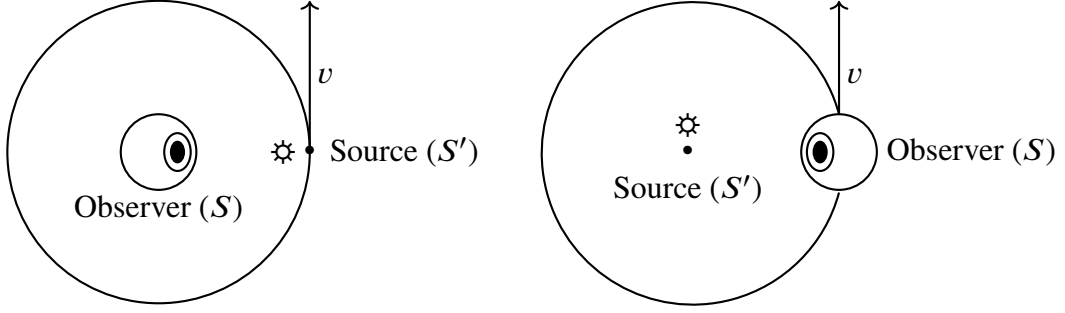
Figure 10: Two examples of transverse motion: Transverse motion in S resulting in redshift (left) and transverse motion in S' resulting in blueshift (right).

4.2.2 Transverse Doppler Effect

With transverse motion, it is necessary to take into account the influence of aberration: The meaning of the direction of movement being at right angles to the vector between the observer and the source is dependent on the frame. Superficial analysis not taking aberration into account might suggest that a planet orbiting a star a perfectly circular orbit would experience Doppler redshift but in fact it will experience blueshift.

Substitution of $\theta = \pi/2$ to (117) yields expression for transverse motion in S

$$\omega = \frac{\omega'}{\gamma} < \omega' \tag{120}$$

However, substitution of $\theta' = \pi/2$ yields $\beta = \cos\theta$ and an expression for transverse motion in S'

$$\omega = \frac{\omega'}{\gamma(1 - \beta^2)} = \gamma\omega' > \omega'. \tag{121}$$

That is, transverse motion from the viewpoint of the observer leads to a redshift and transverse motion from the viewpoint of the source leads to a blueshift. A planet orbiting a star on a circular orbit will experience Doppler blueshift of the starlight and a imaging satellite orbiting a planet will experience (Doppler) redshift (see Figure 10).

4.2.3 Boundary Between Redshift and Blueshift

As shown previously, maximum blueshift and redshift are obtained at angles $\theta = 0°$ and $\theta = 180°$, respectively. The boundary w.r.t. values θ between redshift and blueshift occurs when $\omega = \omega'$ or equivalently

$$\gamma(1 - \beta\cos\theta) = 1 \quad \Leftrightarrow \quad \cos\theta = \frac{1}{\beta}\left(1 - \frac{1}{\gamma}\right). \tag{122}$$

The limit is depicted in Figure 11. When β becomes larger, the region of blueshift gets smaller and converges to a dot when $\beta \to 1$.
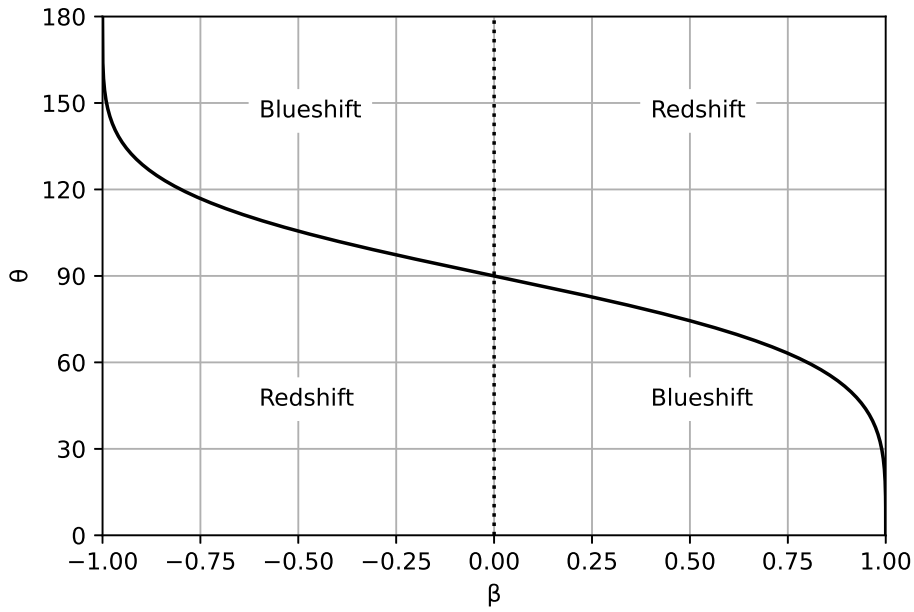
Figure 11: Limit angle between redshift and blueshift. For positive and negative β, the value is the lower and upper limit, respectively of the blueshift for θ.

5 Human Perception

5.1 Perspective Projection

5.1.1 The Camera Frustrum

Perspective projection can be seen as an idealized representation how a camera or the human eye forms a two-dimensional image from light rays received from a three-dimensional scene. Lines-of-sight are considered to converge on a single point, which is considered as the location of the camera. If the image is rectangular, all potentially visible points in the scene are inside an infinite pyramidal shape starting from camera position. Usually, the pyramid is truncated into a **camera frustrum** with **near and far planes** orthogonal to the pointing direction of the camera (see Figure 12) and all points outside the frustrum are discarded (**culling**).

5.1.2 Model, World and View Spaces

Intuitively, the image can be considered to form on the near plane. However, any real-world software implementation typically involves a sequence of coordinate transformations between the world space and normalized device coordinates. In this document, we use standard OpenGL terms and conventions (see e.g. TBA).

Specific objects (e.g. cubes) in a scene might have their geometry defined in an object-specific **local space**, where the object in question is typically placed at the origin. The actual scene inhabits a **world space** into which specific objects are placed according to object-specific mapping defined
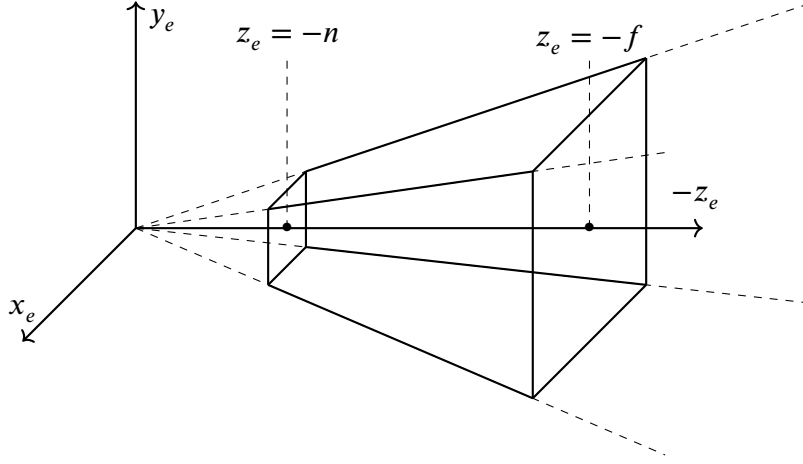
Figure 12: Infinite pyramid truncated into a camera frustrum by near and far planes at $z_e = -n$ and $z_e = -f$, respectively.

by a **model matrix**. Each camera is placed at the origin of the corresponding **view space** pointing to -z-direction and the camera-specific transformation from the world space is defined by a **view matrix**. In the view space, the intersection of the frustrum and the near and far planes correspond to the sets

$$N = [l, r] \times [b, t] \times \{-n\}, \tag{123}$$
$$F = [fl/n, fr/n] \times [fb/n, ft/n] \times \{-f\}, \tag{124}$$

where l, r, b and t refer to left, right, bottom and top coordinate values.

Since the transformations between spaces may involve translation in addition to deformation and rotation, 4x4-matrices operating on the Cartesian coordinates (x, y, z, w) are used, where $w = 1$ in local, world and view spaces. The translation part of such transformation is included in the last column as follows

$$\begin{bmatrix} R_{11} & R_{12} & R_{13} & \Delta x \\ R_{21} & R_{22} & R_{23} & \Delta y \\ R_{31} & R_{32} & R_{33} & \Delta z \\ 0 & 0 & 0 & 1 \end{bmatrix} \begin{bmatrix} x \\ y \\ z \\ 1 \end{bmatrix} = \begin{bmatrix} Rr + \Delta r \\ 1 \end{bmatrix}, \tag{125}$$

where we have denoted $r = [x, y, z]^T$. Note that the matrix R is not applied to the translation part and thus the translation is not a translation in the source coordinate system. For example, if the camera is located at $(p, 1)$ in the world space and points to $+z$-direction, the transformation between the world space coordinates $(x_w, y_w, z_w, w_w = 1)$ to the view coordinates could be

$$\begin{bmatrix} x_e \\ y_e \\ z_e \\ w_e \end{bmatrix} = \begin{bmatrix} -1 & 0 & 0 & p_x \\ 0 & 1 & 0 & -p_y \\ 0 & 0 & -1 & p_z \\ 0 & 0 & 0 & 1 \end{bmatrix} \begin{bmatrix} x_w \\ y_w \\ z_w \\ 1 \end{bmatrix} = \begin{bmatrix} -x_w + p_x \\ +y_w - p_y \\ -z_w + p_z \\ 1 \end{bmatrix}, \tag{126}$$

That is, the translation $(-p_x, -p_y, -p_z)$ in the world space corresponds to a translation $(p_x, -p_y, p_z)$ in the view space.

21

5.1.3 The Clip Space, Projection and Normalized Device Coordinates

In order to draw triangles, lines or points on a screen and clip anything outside the camera frustrum, the coordinates $(x_e, y_e, z_e, w_e = 1)$ from the view space are first transformed into a **clip space** with a **projection matrix**. Then, culling corresponds to discarding vertices with coordinates (x_c, y_c, z_c, w_c) that satisfy

$$\max\left\{|x_c|, |y_c|, |z_c|\right\} > w_c. \tag{127}$$

In the clip space w_c does not necessarily equal to 1. Rather, the clip space is an example of a **homogeneous space**, where the elements $(\alpha x_c, \alpha y_c, \alpha z_c, \alpha)$ are considered equal for all non-zero values of α. After culling, the clip coordinates are therefore transformed to **normalized device coordinates** inside the cube $[-1, 1] \times [-1, 1] \times [-1, 1]$ with

$$(x_n, y_n, z_n) = \left(x_c/w_c, y_c/w_c, z_c/w_c\right). \tag{128}$$

The projection matrix can be derived by first considering **projective plane coordinates** on the near plane and their relation to the normalized device coordinates. If we denote coordinates in view space with $(x_e, y_e, z_e, w_e = 1)$, the intersection between the line to the origin and the near plane is at

$$x_p = \frac{nx_e}{-z_e}, \quad y_p = \frac{ny_e}{-z_e}. \tag{129}$$

The normalized device coordinates x_n, y_n on the near plane linearly map intervals $[l, r]$ and $[b, t]$ to the intervals $[-1, 1]$ and $[-1, 1]$. Thus, we obtain

$$x_n = \frac{2x_p}{r - l} - \frac{r + l}{r - l}, \tag{130}$$

$$y_n = \frac{2y_p}{t - b} - \frac{t + b}{t - b}. \tag{131}$$

Thus, selecting $w_c = -z_e$

$$x_n = \frac{1}{-z_e}\left(\frac{2nx_e}{r - l} + \frac{r + l}{r - l}z_e\right) = \frac{1}{w_e}\left(\frac{2nx_e}{r - l} + \frac{r + l}{r - l}z_e\right) = \frac{x_c}{w_e}, \tag{132}$$

$$y_n = \frac{1}{-z_e}\left(\frac{2ny_e}{t - b} + \frac{t + b}{t - b}z_e\right) = \frac{1}{w_e}\left(\frac{2ny_e}{t - b} + \frac{t + b}{t - b}z_e\right) = \frac{y_c}{w_e}. \tag{133}$$

We also want z_n to obtain values in the interval $[-1, 1]$. Thus, requiring that a linear map $z_c = Az_e + B$ maps $z_e = -n$ and $z_e = -f$ map to $z_c = -n$ and $z_c = f$, respectively, we get

$$z_c = -\frac{f + n}{f - n}z_e - \frac{2fn}{f - n}. \tag{134}$$

In order to check the result, we can compute the corresponding NDC coordinate

$$z_n = \frac{z_c}{-z_e} = \frac{1}{f - n}\left(f + n + \frac{2fn}{z_e}\right). \tag{135}$$

Substituting $z_e = -n$ and $z_e = -f$ then yields $z_n = -1$ and $z_n = 1$, respectively, as expected.

Collecting the above results yields the projection matrix transforming the view coordinates to clip coordinates

$$P = \begin{bmatrix} 2n/(r-l) & 0 & (r+l)/(r-l) & 0 \\ 0 & 2n/(t-b) & (t+b)/(t-b) & 0 \\ 0 & 0 & -(f+n)/(f-n) & -2fn/(f-n) \\ 0 & 0 & -1 & 0 \end{bmatrix} \tag{136}$$

In order to understand the culling criterion (127), note that the projection matrix maps the intersection of each plane with constant z_e with the camera frustrum to

$$[z_e, -z_e] \times [z_e, -z_e] \times \{z_c\} \times \{-z_e\} = [-w_c, w_c] \times [-w_c, w_c] \times \{z_c\} \times \{w_c\}. \tag{137}$$

Any point on the plane outside the frustrum will satisfy (127). On the other hand, if $z_c > w_c$, we get

$$z_c = -\frac{f+n}{f-n}z_e - \frac{2fn}{f-n} > w_c = -z_e \tag{138}$$

from which it easily follows that $z_e < -f$. Similarly, if $z_c < -w_c$, we get

$$z_c = -\frac{f+n}{f-n}z_e - \frac{2fn}{f-n} < -w_c = z_e, \tag{139}$$

which yields $z_c > -n$.

5.1.4 Special Cases of a Projection Matrix

5.2 Human Perception of Color

5.2.1 Human Vision and LMS Color Space

Human vision is limited to the wavelength range between 380 and 700 nm. The perception of color is based on three classes of cone cells on the retina. Each type of cone cell has different **spectral sensitivity**. That is, they are sensitive to different ranges of wavelengths. We can refer to the three classes according to their peak wavelength as long (L), medium (M) and short (S) with peaks at 560, 530 and 420 nm, respectively.

Let $S(\lambda)$ be the **spectral power distribution** (W/m^2/nm) of the light received by the eye. If $\overline{L}(\lambda), \overline{M}(\lambda), \overline{S}(\lambda)$ are cone response functions

$$L = \int_0^\infty S(\lambda)\overline{L}(\lambda)\, d\lambda \tag{140}$$

$$M = \int_0^\infty S(\lambda)\overline{M}(\lambda)\, d\lambda \tag{141}$$

$$S = \int_0^\infty S(\lambda)\overline{S}(\lambda)\, d\lambda, \tag{142}$$

they are called **Color Matching Functions (CMFs)** for the **LMS Color Space**. The cone response functions are normalized so that their maxima are equal to unity (see Figure 13). The triplets (L, M, S) obtained above are called the **tristimulus values**. Two different spectra resulting in the same tristimulus values are called **metamers**.
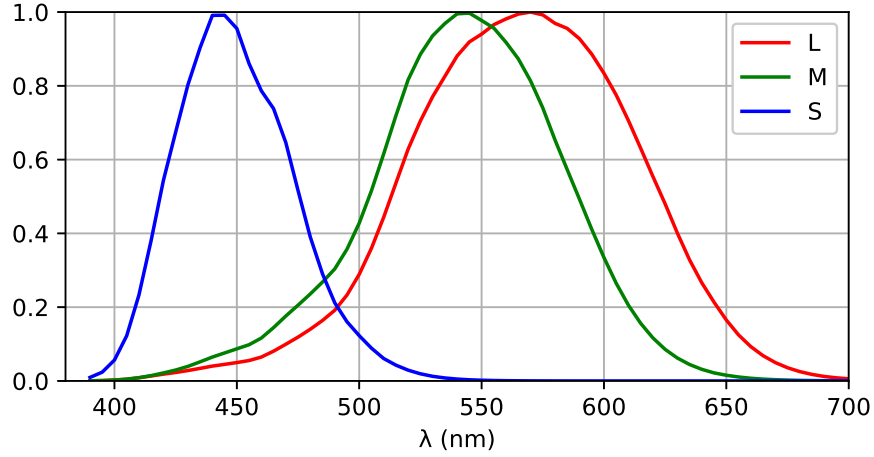
Figure 13: LMS color-matching functions $\overline{L}(\lambda), \overline{M}(\lambda), \overline{S}(\lambda)$.

5.2.2 CIE 1931 Color Spaces and sRGB Encoding

We wish to convert spectrum to 8-bit sRGB values that can be rendered on computer displays. This can be achieved by the use of CIE XYZ color-matching functions and then performing a conversion to SRGB and subsequent quantization. The XYZ color-matching functions are shown in Figure 14 and the corresponding tristimulus values are obtained via the inner products

$$X = \int_0^\infty S(\lambda)\overline{X}(\lambda)\,d\lambda \tag{143}$$

$$Y = \int_0^\infty S(\lambda)\overline{Y}(\lambda)\,d\lambda \tag{144}$$

$$Z = \int_0^\infty S(\lambda)\overline{Z}(\lambda)\,d\lambda. \tag{145}$$

Then, linear sRGB values between in the interval [0, 1] can be obtained via the matrix product

$$\begin{bmatrix} R_{sRGB} \\ G_{sRGB} \\ B_{sRGB} \end{bmatrix} = \begin{bmatrix} 3.2406255 & -1.5372080 & -0.4986286 \\ -0.9689307 & 1.8757561 & 0.0415175 \\ 0.0557101 & -0.2040211 & 1.0569959 \end{bmatrix} \begin{bmatrix} X \\ Y \\ Z \end{bmatrix} \tag{146}$$

and clipping values below 0 and above 1 to 0 and 1, respectively. Before quantization, a "gamma" transfer function is applied

$$C'_{sRGB} = \begin{cases} 12.92\, C_{sRGB}, & C_{sRGB} \leq 0.0031308 \\ 1.055(C_{sRGB})^{(1/2.4)} - 0.055, & C_{sRGB} > 0.0031308 \end{cases} \tag{147}$$

where $C \in \{R, G, B\}$. Finally, the 8-bit quantized values are obtained via

$$\begin{bmatrix} R_{sRGB(8)} \\ G_{sRGB(8)} \\ B_{sRGB(8)} \end{bmatrix} = \text{round}\left(255 \begin{bmatrix} R'_{sRGB} \\ G'_{sRGB} \\ B'_{sRGB} \end{bmatrix}\right) \tag{148}$$
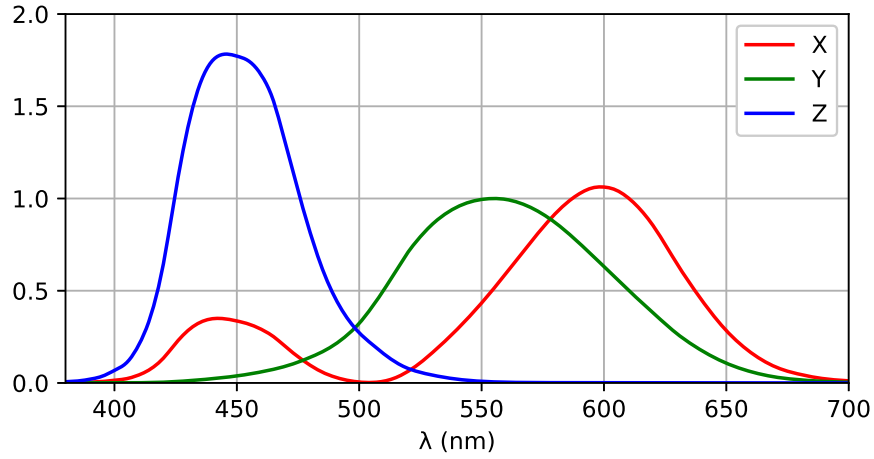
24

Figure 14: The CIE XYZ color-matching functions $\overline{X}(\lambda), \overline{Y}(\lambda), \overline{Z}(\lambda)$.

5.2.3 Example: Visible Wavelength Range

To compute sRGB values corresponding to the visible wavelength range, select for each wavelength λ'

$$S(\lambda) := \frac{1}{2}\delta(\lambda - \lambda'), \tag{149}$$

where δ is the Dirac delta function. The factor is used to avoid saturation in cases where the linear sRGB values become larger than 1. Then,

$$X = \frac{1}{2}\int_0^\infty \delta(\lambda - \lambda')\overline{X}(\lambda)\,d\lambda = \frac{1}{2}\overline{X}(\lambda'), \tag{150}$$

$$Y = \frac{1}{2}\int_0^\infty \delta(\lambda - \lambda')\overline{Y}(\lambda)\,d\lambda = \frac{1}{2}\overline{Y}(\lambda'), \tag{151}$$

$$Z = \frac{1}{2}\int_0^\infty \delta(\lambda - \lambda')\overline{Z}(\lambda)\,d\lambda = \frac{1}{2}\overline{Z}(\lambda'), \tag{152}$$

and application of (146) and (147) yield Figure 15.

6 Spectrum and Radiation

6.1 Basic Radiometry

6.1.1 Black-Body Radiance

Luminosity (also called **radiant flux**) L (W) for a closed surface is an absolute measure of radiated electromagnetic energy per unit time. The luminosity of Sun is denoted $L_\odot$. **Radiance** for a source L_e is the radiant flux from a given surface per unit projected area. That is,

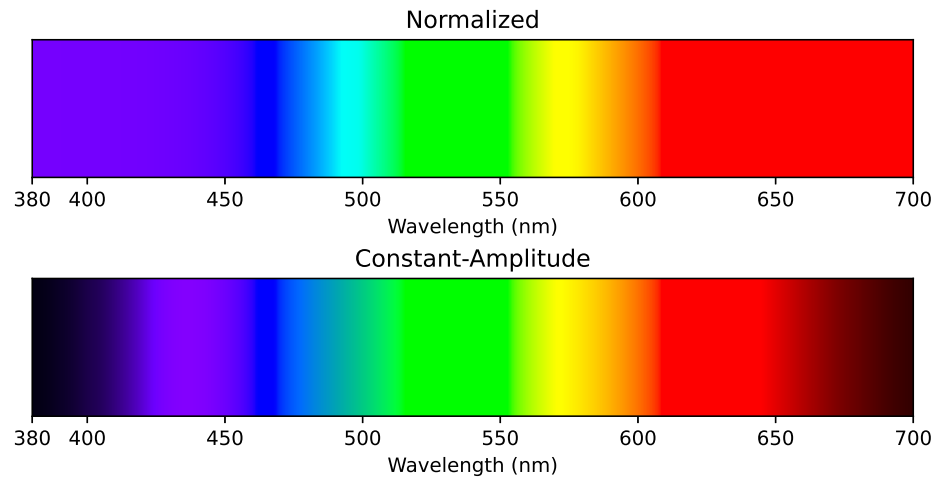$$L_e = \frac{\partial}{\partial\Omega}\frac{\partial L}{\partial A\cos\theta} \tag{153}$$

25

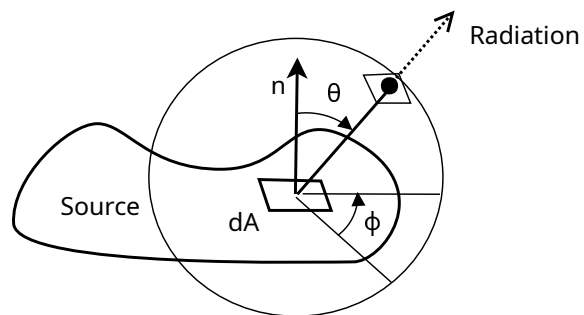**Figure 15:** RGB values obtained with (149) with and without normalization.

Figure 16: Geometry associated to the definition of radiance.

26

where Ω is the solid angle around the surface element dA, A is the area on the source and $\theta \in [0, \pi/2]$ is the angle between the surface normal and the point on the unit sphere (see Figure 16). Projection of an area element dA to the direction θ w.r.t. surface normal is equal to $\cos\theta\, dA$.

Spectral radiance in frequency or wavelength are defined

$$L_{e,\nu} := \frac{\partial L_e}{\partial \nu} \quad\Leftrightarrow\quad L_e = \int_0^\infty L_{r,\nu}(\nu)\, d\nu \tag{154}$$

$$L_{e,\lambda} := \frac{\partial L_e}{\partial \lambda} \quad\Leftrightarrow\quad L_e = \int_0^\infty L_{r,\lambda}(\lambda)\, d\lambda, \tag{155}$$

respectively. Spectral radiance of a **black-body** can be written

$$L_{e,\nu}(\nu) = \frac{2h\nu^3}{c^2}\left[\exp\left(\frac{h\nu}{kT}\right) - 1\right]^{-1} \tag{156}$$

$$L_{e,\lambda}(\lambda) = \frac{2hc^2}{\lambda^5}\left[\exp\left(\frac{hc}{\lambda kT}\right) - 1\right]^{-1}, \tag{157}$$

where $h = 6.62607015 \cdot 10^{-34}\,\mathrm{J \cdot Hz^{-1}}$ is the **Planck's constant** and $k = 1.380649 \cdot 10^{-23}\,\mathrm{J \cdot K^{-1}}$ is the **Bolzmann constant**. To obtain radiance, we integrate over all frequencies

$$L_e = \frac{2h}{c^2}\int_0^\infty \frac{\nu^3\, d\nu}{\exp\left(\frac{h\nu}{kT}\right) - 1} \tag{158}$$

using the substitution $x = h\nu/kT$. Substituting correspondingly $\nu = kT/h\, x$ and $d\nu = kT/h\, dx$, we obtain

$$L_e = \frac{2h}{c^2}\left(\frac{kT}{h}\right)^4 \int_0^\infty \frac{x^3\, dx}{e^x - 1} = \frac{2h}{c^2}\left(\frac{kT}{h}\right)^4 \Gamma(4)\zeta(4), \tag{159}$$

where Γ and ζ are the Gamma and Riemann zeta functions. Substitution of $\Gamma(4) = 6$ and $\zeta(4) = \pi^4/15$ yields

$$L_e = \frac{2\, k^4\pi^4}{15\, h^3 c^2}\, T^4. \tag{160}$$

To obtain the radiant flux, we integrate the radiance over a hemisphere of solid angles and the entire surface

$$L = \oint_A \int_\Omega L_e(\boldsymbol{r}, \theta, \phi) \cos\theta\, d\Omega\, dA \tag{161}$$

where $\boldsymbol{r}$ is a point on the surface element dA. The computation of the integral is simplified by the intependence of radiance (160) from θ and ϕ. For solid angle, we can expand $d\Omega = \sin\theta\, d\theta d\phi$. Thus,

$$L = \oint_A L_e \int_0^{2\pi}\int_0^{\pi/2} \sin\theta\cos\theta\, d\theta\, d\phi\, dA = \pi \oint_A L_e\, dA. \tag{162}$$

If L_e is independent of position on the surface (e.g. due to equal temperature), we obtain

$$L = \pi A L_e. \tag{163}$$

For a black-body, this yields the **Stefan-Boltzmann law**

$$L = \pi A L_e = \frac{2}{15} \frac{k^4 \pi^5}{h^3 c^2} A T^4 = \sigma A T^4, \tag{164}$$

where the **Stefan-Boltzmann constant**

$$\sigma = \frac{2k^4 \pi^5}{15h^3 c^2} = 5.670374419 \cdot 10^{-8} \text{ W} \cdot \text{m}^{-2} \cdot \text{K}^{-4}. \tag{165}$$

6.1.2 Wien's Displacement Law

To obtain peak frequency of the black body radiance as a function of temperature, we derivate (156) w.r.t. frequency

$$\frac{\partial L_{e,\nu}}{\partial \nu} = \frac{6h\nu^2}{c^2} \left[\exp\left(\frac{h\nu}{kT}\right) - 1 \right]^{-1} - \frac{2h^2 \nu^3}{c^2 kT} \exp\left(\frac{h\nu}{kT}\right) \left[\exp\left(\frac{h\nu}{kT}\right) - 1 \right]^{-2} = 0. \tag{166}$$

Substitution of $x = h\nu/kT$ yields

$$x = 3(1 - e^{-x}), \tag{167}$$

which admits numerical solution

$$x = \frac{h\nu}{kT} \approx 2.821439372122078893 \tag{168}$$

Thus, the black-body radiance obtains it's peak at the frequency

$$\nu_{peak} = \frac{kT}{h} x \approx 5.878925757646824946 T \cdot 10^{10} \text{ Hz} \cdot \text{K}^{-1} \tag{169}$$

To obtain peak wavelength of the black body radiance as a function of temperature, we derivate (157) w.r.t. wavelength

$$\frac{\partial L_{e,\lambda}}{\partial \lambda} = -\frac{10hc^2}{\lambda^6} \left[\exp\left(\frac{hc}{\lambda kT}\right) - 1 \right]^{-1} + \frac{2h^2 c^3}{\lambda^7 kT} \exp\left(\frac{hc}{\lambda kT}\right) \left[\exp\left(\frac{hc}{\lambda kT}\right) - 1 \right]^{-2} = 0. \tag{170}$$

Substitution of $y = hc/\lambda kT$ yields

$$y = 5(1 - e^{-y}), \tag{171}$$

which admits numerical solution

$$y = \frac{hc}{\lambda kT} \approx 4.965114231744276303. \tag{172}$$

Thus, the black-body radiance obtains it's peak at the wavelength

$$\lambda_{peak} = \frac{hc}{ky} \frac{1}{T} \approx 2.897771955/T \cdot 10^{-3} \text{ m} \cdot \text{K}. \tag{173}$$
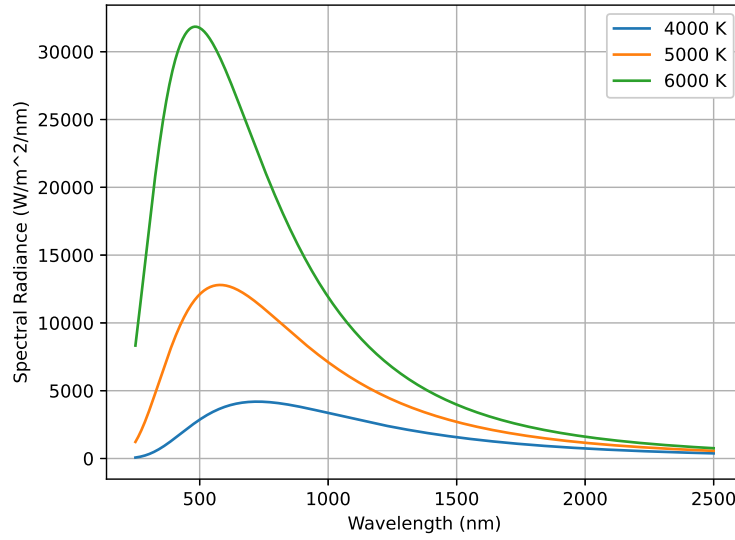
Figure 17: Three examples of black-body spectra.

The equation (173) is called the **Wien's displacement law** and is usually written in terms of the constant of proportionality $b = hc/ky$ called the **Wien's displacement constant**. Note that when the blackbody radiance is expressed as a function of wavelength and frequency, the peak occurs at a different frequency in the sense that we cannot transform between the peak wavelength and peak frequency with the relation $\lambda v = c$.

Three examples of black-body spectra are shown in Figure 17. Substitution of $T = 4000\text{K}, 5000\text{K}$ and 6000K yields $\lambda_{max} = 724.44\,\text{nm}, 579.55\,\text{nm}$ and $482.96\,\text{nm}$, respectively. The increasing spectral radiance of the curves seems consistent with (164) since $5^4/4^4 \approx 2.44$ and $6^4/5^4 \approx 2.49$.

6.1.3 Effective Temperature and Color

Visual perception of black-body as a function of its **effective temperature** is easily obtained using the computation in section 5.2.2. In Figure 18, SRGB values for black-bodies are displayed for a temperature range. The XYZ-values have been normalized before SRGB conversion by division with $\max\{X, Y, Z\}$.

6.2 Lorentz Transformations

It's somewhat likely that portion of details in this section are wrong.
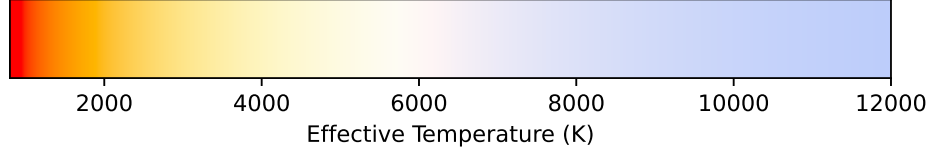
29

Figure 18: Visual perception of color for black-bodies at temperatures between 800 K and 12000 K.

6.2.1 Plane Waves and Intensity

Intensity I associated to electromagnetic wave is the time-average of the **Poynting vector** S. That is,

$$I = |\langle S \rangle| = \frac{1}{\mu_0} |\langle E \times B \rangle|, \tag{174}$$

where μ_0 is the permeability of vacuum $\mu_0 = 1.25663706127 \cdot 10^{-6} \, \text{N} \cdot \text{A}^{-2}$. Suppose inertial frame S' is moving in the +x direction w.r.t. inertial frame S with velocity v. Then, the electric field E and the magnetic flux density B vectors transform [7]

$$E'_{||} = E_{||}, \tag{175}$$
$$E'_{\perp} = \gamma \left(E_{\perp} + v \times B \right), \tag{176}$$
$$B'_{||} = B_{||}, \tag{177}$$
$$B'_{\perp} = \gamma \left(B_{\perp} - \frac{1}{c^2} v \times E \right), \tag{178}$$

where we have used $||$ and $\perp$ to denote components parallel and perpendicular to the motion. The velocity can be expressed $v = v\hat{x}$.

Consider a linearly polarized plane wave solution with propagation direction at an angle θ w.r.t. v:

$$E = E_0 \left(\cos \theta \, \hat{y} + \sin \theta \, \hat{x} \right), \tag{179}$$
$$B = E_0/c \, \hat{z}, \tag{180}$$

where we have left out the $\cos(k \cdot r - \omega t + \delta)$ for brevity. Application of the Lorentz transformation (175)-(178) yields the fields in S':

$$E'_{\perp} = \gamma E_0 \left(\cos \theta - \beta \right) \hat{y}, \tag{181}$$
$$E'_{||} = E_0 \sin \theta \, \hat{x}, \tag{182}$$
$$B'_{\perp} = \gamma E_0/c \, (1 - \beta \cos \theta) \hat{z}, \tag{183}$$
$$B'_{||} = 0. \tag{184}$$

30

Now the Poynting vector can be computed

$$\frac{1}{\mu_0} \boldsymbol{E}' \times \boldsymbol{B}' \;=\; \frac{1}{\mu_0} \boldsymbol{E}'_{\parallel} \times \boldsymbol{B}'_{\perp} + \frac{1}{\mu_0} \boldsymbol{E}'_{\perp} \times \boldsymbol{B}'_{\perp} \tag{185}$$

$$= \; \frac{E_0^2}{\mu_0}(1 - \beta \cos\theta) \left\{ (\sin\theta\,\hat{\mathbf{x}}) \times \left(\frac{\gamma}{c}\,\hat{\mathbf{z}}\right) + \left[\gamma(\cos\theta - \beta)\hat{\mathbf{y}}\right] \times \left(\frac{\gamma}{c}\hat{\mathbf{z}}\right) \right\} \tag{186}$$

$$= \; \frac{E_0^2 \gamma}{c\mu_0}(1 - \beta \cos\theta)\left[-\sin\theta\,\hat{\mathbf{y}} + \gamma(\cos\theta - \beta)\,\hat{\mathbf{z}}\right]. \tag{187}$$

Squaring the expression in square brackets yields

$$\sin^2\theta + \frac{\cos^2\theta - 2\beta\cos\theta + \beta^2}{1 - \beta^2} \;=\; \frac{\sin^2\theta - \beta^2\sin^2\theta + \cos^2\theta - 2\beta\cos\theta + \beta^2}{1 - \beta^2} \tag{188}$$

$$= \; \gamma^2(1 - 2\beta\cos\theta + \beta^2\cos^2\theta) \tag{189}$$

$$= \; \gamma^2(1 - \beta\cos\theta)^2. \tag{190}$$

Substitution back to (187) and application of (117), yields

$$\frac{1}{\mu_0}|\boldsymbol{E}' \times \boldsymbol{B}'| = \frac{E_0^2 \gamma^2}{c\mu_0}(1 - \beta\cos\theta)^2 = \left(\frac{\omega'}{\omega}\right)^2 \frac{1}{\mu_0}|\boldsymbol{E} \times \boldsymbol{B}| \tag{191}$$

Thus, the intensity of plane waves transforms between frames proportionally to the square of frequency, where the frequency ratio follows from the equation (117) for the relativistic Doppler effect:

$$\boxed{\frac{I'}{I} = \left(\frac{\omega'}{\omega}\right)^2 = \gamma^2(1 - \beta\cos\theta)^2.} \tag{192}$$

6.2.2 Wave Four-Vector

Consider again a plane wave in S propagating to a direction that makes the angle θ with the +x direction in S. Then, if the frame S' moves with velocity v into the +x direction w.r.t. S, the wave four-vectors

$$k \;=\; (\omega/c, k\cos\theta, k\sin\theta, 0), \tag{193}$$

$$k' \;=\; (\omega'/c, k'\cos\theta', k'\sin\theta, 0) \tag{194}$$

in S and S' can be related by the inverse Lorentz transformation [8]

$$\begin{bmatrix} \omega/c \\ k\cos\theta \\ k\sin\theta \\ 0 \end{bmatrix} = \begin{bmatrix} \gamma & \gamma\beta & 0 & 0 \\ \gamma\beta & \gamma & 0 & 0 \\ 0 & 0 & 1 & 0 \\ 0 & 0 & 0 & 1 \end{bmatrix} \begin{bmatrix} \omega'/c \\ k'\cos\theta' \\ k'\sin\theta' \\ 0 \end{bmatrix} = \begin{bmatrix} \gamma(\omega'/c + \beta k'\cos\theta') \\ \gamma(\beta\omega'/c + k'\cos\theta') \\ k'\sin\theta' \\ 0 \end{bmatrix}. \tag{195}$$

This transformation is a treasure trove of useful information: The first row implies

$$\omega = \gamma(\omega' + \beta k'c\cos\theta') = \gamma\omega'(1 + \beta\cos\theta'), \tag{196}$$

31

which is equivalent to the relativistic Doppler effect in (117). The ratio of the third and second rows can be expanded

$$\tan \theta = \frac{k' \sin \theta'}{\gamma(\beta \omega'/c + k' \cos \theta')} = \frac{\sin \theta'}{\gamma(\cos \theta' + \beta)} = \frac{\tan \theta'}{\gamma(1 + \beta \sec \theta')}, \tag{197}$$

which is the relativistic aberration formula (10). The third row is equivalent to the y-component of (117) for the wave vector and by using the relation $k = \omega/c$ can be converted into an another useful relation

$$\omega \sin \theta = \omega' \sin \theta'. \tag{198}$$

The ratio of the second and first rows also yields the relation

$$\cos \theta = \frac{\beta \omega'/c + k' \cos \theta'}{\omega'/c + \beta k' \cos \theta'} = \frac{\cos \theta' + \beta}{1 + \beta \cos \theta'}. \tag{199}$$

6.2.3 Headlight Effect for Monochromatic Waves

Consider monochromatic radiation source fixed in S' that radiates with equal power to all directions. Suppose again also that the S' moves w.r.t. S to +x direction with velocity v. Let θ' be the angle in S' w.r.t. direction of velocity. We want to find the dependence of radiated power density in S on the angle θ and the solid angle Ω. The luminosity is dependent of the frame. In fact, it diverges towards infinity as the speed of the source w.r.t. observer converges towards the speed of light. However, if the source emits a (large) fixed number N of particles uniformly to all direction over some specific period, it makes sense to ask what is the dependence of the density of expected number of particles on θ and Ω.

The number of particles per unit angle to the directions $(\theta', \theta' + d\theta')$ can be written

$$\frac{dN}{d\theta'} = N \frac{2\pi r \sin \theta'}{4\pi r^2} r = \frac{N}{2} \sin \theta'. \tag{200}$$

Now, we want to find an expression for the expected number of particles per unit angle in S. By chain rule, this should be equal to

$$\frac{dN}{d\theta} = \frac{dN}{d\theta'} \frac{d\theta'}{d\theta}. \tag{201}$$

From (199), we can solve

$$\cos \theta' = \frac{\cos \theta - \beta}{1 - \beta \cos \theta}. \tag{202}$$

Differentiating w.r.t. θ, yields

$$-\sin \theta' \frac{d\theta'}{d\theta} = \frac{-\sin \theta(1 - \beta \cos \theta) - (\cos \theta - \beta)\beta \sin \theta}{(1 - \beta \cos \theta)^2} \tag{203}$$

$$= \frac{-\sin \theta + \beta \sin \theta \cos \theta - \beta \sin \theta \cos \theta + \beta^2 \sin \theta}{(1 - \beta \cos \theta)^2} \tag{204}$$

$$= \frac{-\sin \theta(1 - \beta^2)}{(1 - \beta \cos \theta)^2}. \tag{205}$$

Thus, we obtain

$$\frac{d\theta'}{d\theta} = \frac{\sin\theta}{\sin\theta'}\frac{1-\beta^2}{(1-\beta\cos\theta)^2} \tag{206}$$

Combination with (200), yields

$$\frac{dN}{d\theta} = \frac{dN}{d\theta'}\frac{d\theta'}{d\theta} = \frac{N}{2}\sin\theta\frac{1-\beta^2}{(1-\beta\cos\theta)^2}. \tag{207}$$

In S' the number of particles per solid angle is uniformly

$$\frac{dN}{d\Omega'} = \frac{N}{4\pi}, \tag{208}$$

where 4π is the solid angle of the entire sphere. To obtain corresponding expression w.r.t. Ω, we first note the relationship between solid angles and θ

$$\frac{d\theta}{d\Omega} = \frac{1}{2\pi\sin\theta}. \tag{209}$$

Application of the chain rule now yields

$$\frac{dN}{d\Omega} = \frac{dN}{d\theta}\frac{d\theta}{d\Omega} = \frac{N}{2}\sin\theta\frac{1-\beta^2}{(1-\beta\cos\theta)^2}\frac{1}{2\pi\sin\theta} = \frac{N}{4\pi}\frac{1}{\gamma^2(1-\beta\cos\theta)^2} \tag{210}$$

and application of relativistic Doppler effect (117) leads to the desired result

$$\boxed{\frac{dN}{d\Omega} = \frac{N}{4\pi}\left(\frac{\omega}{\omega'}\right)^2 = \left(\frac{\omega}{\omega'}\right)^2\frac{dN}{d\Omega'}} \tag{211}$$

That is, the number of particles per unit solid angle transforms according to the squared ratio of frequencies from the relativistic Doppler effect. However, note that this derivation didn't involve EM radiation to which one could associate frequency. To obtain a transformation for the radiated power density per unit solid angle, we can use the relationship (192) for the intensity of plane waves in the two frames. If the preceding argument describes the "number" of plane waves associated to specific power the intensity relates the power of each plane wave.

This suggests that power density w.r.t. solid angle satisfies

$$\boxed{\frac{dL}{d\Omega} = \left(\frac{\omega}{\omega'}\right)^4\frac{dL'}{d\Omega'}.} \tag{212}$$

6.2.4 Black-Body Radiance

For an observer moving at relativistic speeds, the perceived color of black-body sources can be significantly influenced by the Doppler effect. However, since the black-body radiation is not monochromatic but consists of a continuous spectrum, the computation of the Doppler effect is no longer trivial. In a continuous spectrum, we do not expect a radiance that transforms proportionally to

33

fourth power of the frequency: If the Doppler effect indicates a ratio ω/ω' ratio of frequencies between S and S' spectrum in the range $[\omega', \omega' + \Delta']$ in S' will correspond to spectrum in the range $[\omega, \omega + (\omega/\omega')\Delta']$ in S. This suggests that radiance transforms instead to the third power.

In S', we have spectral radiance

$$L_{e,v'}(v') = \frac{2hv'^3}{c^2} \left[\exp\left(\frac{hv'}{kT'}\right) - 1 \right]^{-1}. \tag{213}$$

From superficial interpration of [5], [6], it seems that the argument to the exponential term transforms according to an **effective temperature** so that

$$T = \frac{T'}{\gamma(1 - \beta\cos\theta)} = \left(\frac{\omega}{\omega'}\right)T'. \tag{214}$$

The amplitude term is replaced with one with third power of the Doppler-transformed frequency.

6.3 Stars

6.3.1 Spectrum of Stars

The electromagnetic spectrum of stars essentially follow the blackbody spectrum complicated slightly by absorption and emission lines. However, for visual effects discussed in this section, they can be approximated as ideal black-bodies. Spectral classification of the star essentially determines to the selection of an **effective temperature** T'_{eff} used for the black-body spectrum in the rest frame of the star.

6.3.2 Observed Color

To compute the color of a distant star observed by an observer in relative motion, we simply compute the effective temperature T_{eff} of the star in the frame of the observer using (214). When the observer is travelling directly towards the star in longitudal motion, this corresponds to the selection of $\theta = 0$. Figure 19 shows the observed color for a range of effective temperatures (in S') for an observer moving with velocity β. Figure 20 shows the observed color for a range of angles θ w.r.t. the direction of motion for a black-body with the effective temperature $T' = 5778$ K of the Sun.

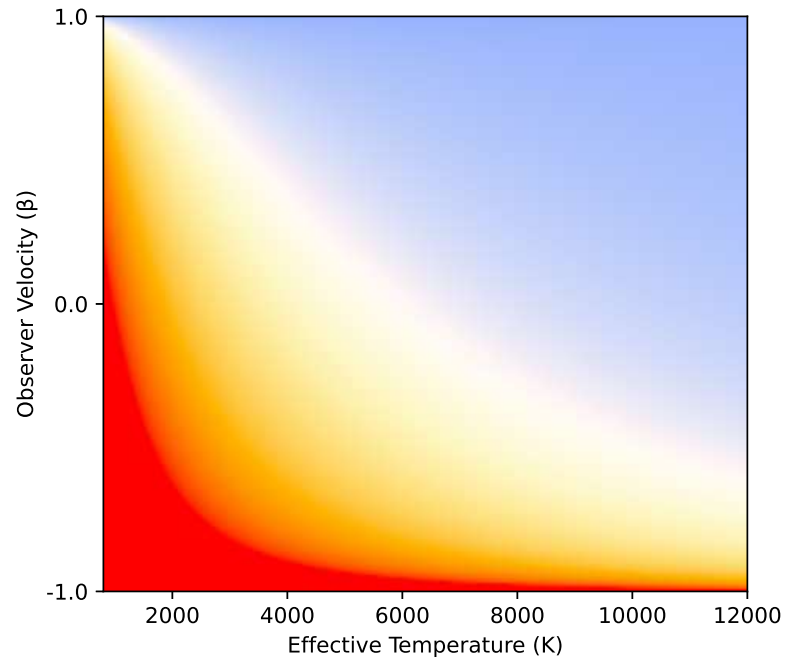### 6.3.3 Observed Spectral Power Distribution

Figure 19: Observed color of a black-body with given effective temperature for an observer in longitudal motion w.r.t. source.
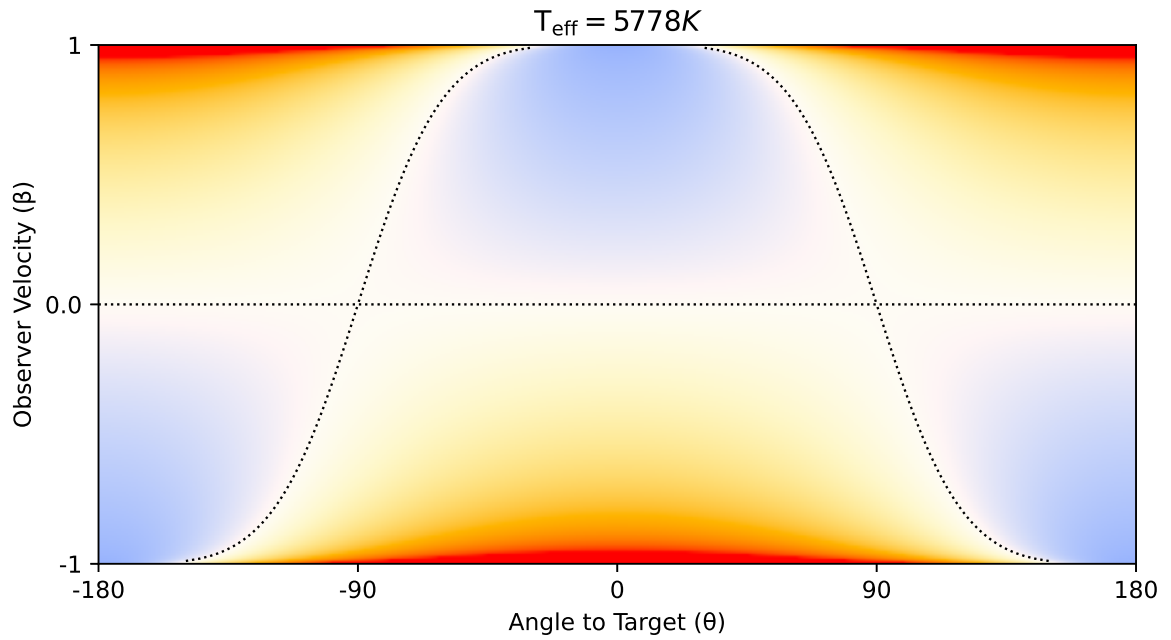

Figure 20: Observed color of a black-body approximating the Sun at an angle θ w.r.t. the direction of motion.

7 Visual Effects at Relativistic Speeds

7.1 Deformation

7.1.1 Grid Deformation

7.1.2 Solid Objects

7.2 Brightness

7.2.1 Headlight Effect

References

[1] Lightman, Press, Price, Teukolsky, Problem Book in Relativity and Gravitation, Princeton University Press, 2017.

[2] Urban, Seidelmann, Explanatory Supplement to the Astronomical Alamanac, 3rd Edition, University Science Books, 2012.

[3] CIE 1931 2-deg XYZ CMFs, Colour & Vision Research Laboratory, Institute of Opthalmology, University College London. Available at `http://cvrl.ioo.ucl.ac.uk/cie.htm`.

[4] Walker, Saunders, Hattenburg, Spectral Radiance Calibrations, NBS Special Publication 250-1, 1987.

[5] Ford, O'Connell, Lorentz transformation of blackbody radiation, Phys. Rev. E 88, 2013.

[6] Yurtsever, Wilkinson, Limits and Signatures of Relativistic Spaceflight, Acta Astronautica, Vol. 142, 2018

[7] Griffiths, Introduction to Electrodynamics, 3rd Edition, Pearson, 2008.

[8] Steane, Symmetry and Relativity, Lecture Notes, Oxford University, 2011. Available at `https://users.physics.ox.ac.uk/~Steane/teaching/lecture_course.html`.